Direct Observation of Rectified Motion of Vortices in a Niobium Superconductor

Yoshihiko Togawa,[1,*] Ken Harada,[1,2] Tetsuya Akashi,[3] Hiroto Kasai,[1,2] Tsuyoshi Matsuda,[1,4] Franco Nori,[1,5] Atsutaka Maeda,[1,6] and Akira Tonomura[1,2]

[1]*Frontier Research System, the Institute of Physical and Chemical Research (RIKEN), Hatoyama, Saitama 350-0395, Japan*
[2]*Advanced Research Laboratory, Hitachi, Ltd., Akanuma, Hatoyama, Saitama 350-0395, Japan*
[3]*Hitachi Instruments Service Co.,Ltd., Yotsuya, Shinjyuku-ku, Tokyo 160-0004, Japan*
[4]*Hitachi Science Systems, Ltd., Ishikawa, Hitachinaka, Ibaraki 312-0057, Japan*
[5]*Department of Physics, The University of Michigan, Ann Arbor, Michigan 48109-1120, USA*
[6]*Department of Basic Science, The University of Tokyo, Komaba, Meguro-ku, Tokyo 153-8902, Japan*
(Received 10 September 2004; published 17 August 2005)

Using Lorentz microscopy to directly image vortices, we investigate vortex motion control and rectification in a niobium superconductor. We directly observe a net motion of vortices along micro-fabricated channels with a spatially asymmetric potential, even though the vortices were driven by an oscillatory field. By observing the individual motion of vortices, we clarify elementary processes involved in this rectification. To further demonstrate the ability to control the motion of vortices, we created a tiny vortex ‘‘racetrack’’ to monitor the motion of vortices in a closed circuit channel.

DOI: 10.1103/PhysRevLett.95.087002 PACS numbers: 74.25.Qt, 05.60.−k, 74.70.Ad, 85.25.Am

Brownian motors are attracting considerable attention because these can be used to control the motion of tiny particles [1], even in the absence of dc drives. The idea that oscillating forces (or random forces, e.g., thermal fluctuations) could generate a net motion along one direction has inspired a novel generation of devices in a wide range of fields, from microfluidics to electron devices operating either in the ballistic or tunneling regimes [1]. Regarding vortex matter in superconductors, vortex motion control is being explored in a variety of systems [2–8]. For many device applications, including SQUIDs, vortex motion causes noise that degrades their performance. Thus, it is advantageous to selectively remove undesirable vortices and precisely control their motion.

Theoretical studies have proposed different ways to rectify the motion of vortices in a superconductor [2–6]. Most cases consider a spatially asymmetric potential in the sample, and an externally applied ac drive. An asymmetry of the pinning force (critical current) with regard to a reversal of the dc driving current in superconducting foils with a series of asymmetric surface microgrooves was observed in Ref. [9]. Recently, a remarkable reversible (i.e., the direction of net dc motion could also be controlled) rectifier was obtained in Ref. [8] using a hybrid magnetic-superconducting system. However, none of the experiments done so far could monitor the individual motion of vortices. A microscopic understanding of the vortex dynamics in this asymmetric system requires the use of direct imaging techniques.

The aim of this study is to investigate the microscopic individual motion of vortices in superconducting ratchets by direct imaging via Lorentz microscopy [10]. An advantage of our method is that it allows the possibility of finding ways to improve the performance of this device based on the knowledge obtained by the direct observation of the individual vortices moving inside the fabricated potential. Rectified motion of vortices was observed via video (see, e.g., [11]) in the asymmetric potential under a periodically oscillating magnetic field. From these direct observations, the elementary processes of the rectification were clarified. As an example to further demonstrate the ability to control vortex motion, we built a very tiny ‘‘vortex race track’’ (i.e., a channel shaped as a closed circuit) and observed the motion of vortices while navigating the ‘‘obstacles’’ or ‘‘bumps’’ in the channel.

Our method of fabricating the asymmetric potential in the sample was focused gallium ion beam (FIB) irradiation [12,13]. Figure 1(a) shows one of the irradiation patterns, which includes 832 irradiated points of pin sites in $21 \times 24\ \mu m^2$. This pattern can be regarded as a sequence of unirradiated arrow-shaped wedged cages, that work as microscopic ‘‘funnels’’ for vortex motion [3]. Channels with opposite direction were also fabricated side-by-side in order to study alternating rows of oppositely oriented unidirectional motions. The matching field of a vortex triangular array, with a period of 0.6 μm, was 67 Oe. Electron microscopy revealed that the typical diameter of the irradiated defects was 100 nm.

The potential energy landscape, due to the vortex-vortex long-range Pearl repulsive interaction [14], was calculated, where each dot in Fig. 1(a) was occupied by one vortex. The vortices move in an asymmetric periodic potential energy U_{vv}, as shown in the 1D cut of U_{vv} in Fig. 1(b). The lower energies of the potential form a 2D periodic arrow-shaped spatially asymmetric pattern. When unpinned vortices in the cage are subject to a driving force directed downward, they can be guided toward the long side-wing ‘‘pocket’’ areas of the arrows and accumulate there. However, vortices driven upward are ‘‘funneled’’ toward the next cage. This pattern rectified vortex motion inside the channels [11].

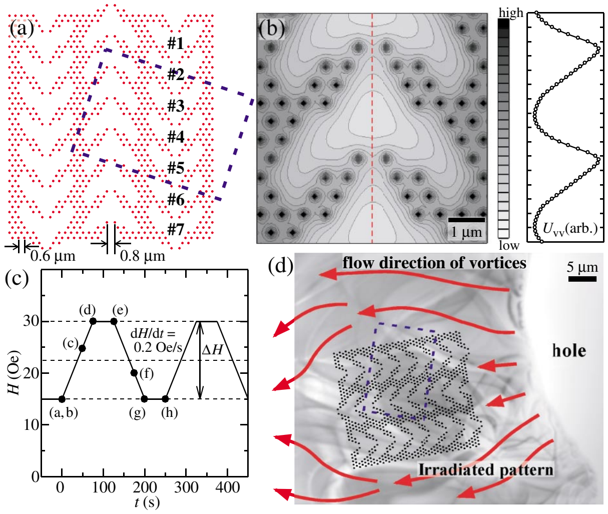

FIG. 1 (color). (a) Pinning site locations (red dots) of the FIB-irradiated sample. For clarity, each cage (with no pins) in a downward channel was numbered (no. 1 to no. 7). (b) Calculated equipotential contours (arbitrary units) produced by vortices pinned at the periodic array of red dots shown in (a), together with a 1D cut U_{vv} along the red vertical line in the contour map. The gradients of the 1D cut U_{vv} on the steep and on the smooth branches of the profile are 5.6×10^{-5} and 3.1×10^{-5} N/m per unit length, respectively. (c) A cycle of H versus time. The solid circles labeled by letters (a to h) indicate the corresponding fields for the snapshots shown in Fig. 2. (d) TEM image of a Nb film showing part of the sample, the irradiated pattern, and schematic arrows for the flow of vortices. The dashed blue squares in (a) and (d) show the field of view in Fig. 2.

Vortices were driven by changing the applied magnetic field $H(t)$ as shown in Fig. 1(c): oscillating H, with a fixed amplitude, ΔH, and a constant ramping rate, $\mathrm{d}H/\mathrm{d}t$, of $\sim$0.2 Oe/s in a temporally symmetric manner. The motion of the vortices was monitored using video (30 frames/s) by Lorentz microscopy using the 1 MV field emission electron microscope [15].

The samples were Niobium (Nb) thin films. In the middle of the sample, an internal hole was produced by chemical etching. Then, the sample was cut and the hole was connected to the outside so that vortices smoothly entered from an edge of the hole into a central part of the film with increasing H. Several irradiated areas with uniform thickness of $\sim$100 nm, near the hole (with vortices flowing dominantly in the direction parallel to the channels in the irradiated pattern) were chosen for observation, as shown in Fig. 1(d).

Figures 2(a) and 2(b) show Lorentz image snapshots of vortices taken at 15 Oe and 6.9 K. From these figures, three different regions can be recognized. One is a pin-free region on the right side (slightly up) of the field of the view. The second region is a channel formed by a series of arrow-shaped wedged cages which are directed toward the southeast direction. The leftmost channel is directed northwest. As an initial state, each irradiated defect must be filled with one vortex so that the irradiated pattern works as a spatially asymmetric potential. Thus, the initial state was prepared via field cooling: the temperature was decreased to below $T_c = 9.2$ K, with $H = 100$ Oe, which is above the first matching field (67 Oe). Then H was decreased to 15 Oe, with the pinned vortices (trapped in the periodic array of defects) remaining fixed. At 15 Oe, 832 vortices were pinned at the irradiated defects, and about 333 vortices were distributed both inside the channel and outside the irradiated region, inside a $40 \times 40\ \mu\mathrm{m}^2$ square. Corresponding magnetic field densities B were 33 G for the irradiated area and 6 G nearby it, respectively. In this situation, with increasing H above 15 Oe, vortices were

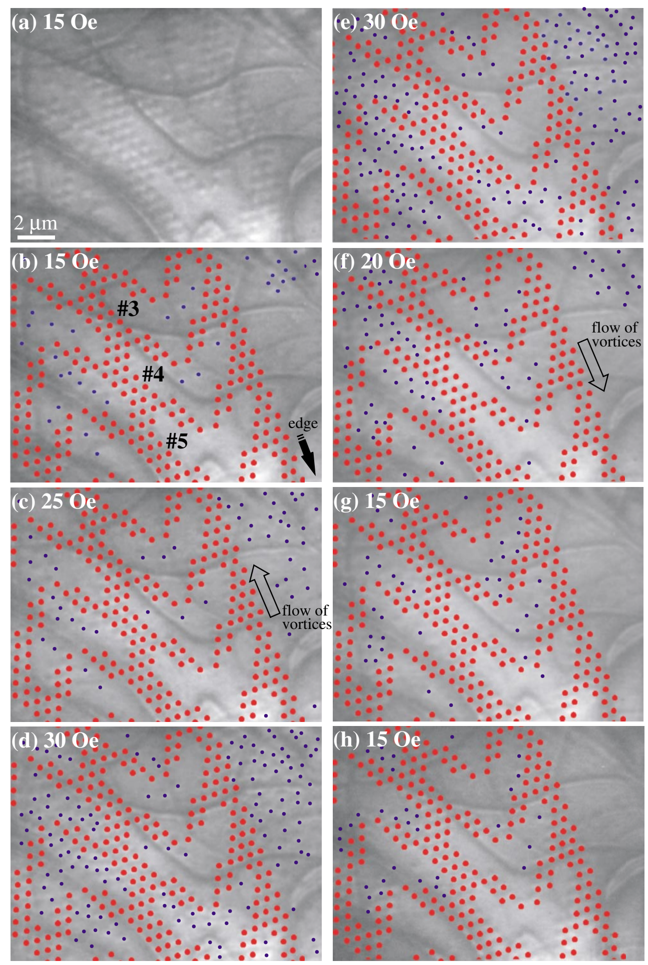

FIG. 2 (color). Sequence of Lorentz image snapshots of moving vortices in a period of the ac applied magnetic field [shown in Fig. 1(c)] at 6.9 K. Pinned and unpinned vortices are represented by red and blue circles, respectively, in (b)–(h). (a) and (b) are the same snapshot. With increasing H, vortices flow upward. (b)–(d) Increasing H for 15, 25, and 30 Oe. (e)–(g) Decreasing H at 30, 20, and 15 Oe. (h) Fixing H at 15 Oe for 50 s. Each of these micrographs was extracted from video frames. Each cage in the downward channel was numbered, as in Fig. 1(a). Arrows indicate the directions toward the edge of the sample, and the flow of vortices.

driven inward owing to a field gradient, dB/dx, created by a gradient of vortex density outside the irradiated area.

Figures 2(c) and 2(d) show snapshots of moving vortices when increasing H from 25 to 30 Oe. Figures 2(e)–2(g) were taken when decreasing H to 30, 20, and 15 Oe, respectively. Outside the pinning (red) region, the number of unpinned vortices increased or decreased with increasing or decreasing H. This occurred because vortices were smoothly pushed inward (outward) from (to) the edge of the sample with increasing (decreasing) H. Therefore, no net motion of vortices occurred outside the potential during an H cycle, as was naturally expected for the pin-free region. In short, $\langle dB/dx \rangle_t = 0$ was satisfied around this region in an H cycle.

The situation was rather different inside the arrow-shaped channels. When H increased, a steady penetration of vortices from the bottom cage toward the upper cages was observed in the upward [leftmost in Figs. 2(b)–2(d)] channel. Vortices behaved in a different way in the downward channel: Vortices first penetrated through the potential energy cage no. 7 [marked in Fig. 1(a)] eventually reaching cage no. 5; 15 vortices were found in cage no. 5, as shown in Figs. 2(d) and 2(e). In addition, when increasing H, vortices outside the irradiated area reached its top side, and some penetrated into the downward channel through cage no. 1, toward cage no. 2. Indeed, four vortices are visible in cage no. 2 in Figs. 2(d) and 2(e). However, it is noteworthy that the number of vortices remained fixed in cages no. 3 and no. 4, with increasing H.

When decreasing H, unpinned vortices in the downward channel went down through the channel and most of them were finally expelled from the bottom cage no. 7, toward the outside of the irradiated region. Notice that the number of vortices in cage no. 5 changes from 15 to 1, when H was decreased by just 10 Oe, in short, from Fig. 2(e) to 2(f). Vortices did not escape through cage no. 1 in the upward direction, and also did not penetrate into cage no. 1 from the outside. Since vortices did not enter cages no. 3 and no. 4 from the bottom, when increasing H, and some vortices in cages no. 1 through no. 4 went down through cage no. 4 with decreasing H, the net number of rectified vortices transported downward was nonzero in an H cycle. Therefore, we obtained direct microscopic evidence for the rectification of vortices in this spatially asymmetric structure. In the upward channel, most vortices trapped in the top and the neighboring cages escaped upward toward the outside (i.e., vortex motion was rectified upward) when increasing H. When decreasing H, vortices began to go down through the lower cages toward the outside. However, several vortices were still trapped in the pockets in the upward channel, as shown in Fig. 2(h). They were pushed upwards, through the channel, when increasing H, and finally rectified upwards after several cycles of H.

The role of each cage in the downward channel is summarized as follows. Vortices penetrated and remained trapped in cages no. 1 and no. 2 with increasing H and were transported downward when H decreased. In this sense, cages no. 1 and no. 2 worked as a reservoir of vortices to be rectified. The rectification occurred through cages no. 3 and no. 4. Cages no. 5 through no. 7 worked as a buffer to prevent vortices from penetrating from the bottom throughout the channel, which is caused when a large difference appears in the vortex density inside and outside the channel. Here, the number of cages in each channel was limited to seven. When increasing the number of cages, we expect the rectification to mostly occur in the (longer) central part of the channel.

Similar rectified motion was observed when the amplitude ΔH of the oscillation of H was varied from 5 to 25 Oe, with the minimum value of H fixed at 15 Oe. Figure 3 shows the net number of vortices N_v rectified downward from cage no. 3 to no. 4, versus ΔH, in a single cycle of the periodically changing H. N_v was obtained by analyzing the video. N_v increases monotonically with increasing ΔH, as in the low-T limit of the theoretical Fig. 4 in [3]. If we had many parallel channels pointing upward, then the total number of rectified vortices would be much larger. A parallel-channels version of our device has recently been made using asymmetric pores in a silicon membrane acting as massively parallel ratchets [16]. We used extremely low frequencies, below 0.01 Hz. For example, in Fig. 1(c), a period of each cycle was 250 s. Vortices intermittently rearranged themselves throughout the cycle, until quasiequilibrium configurations were reached at both constant maximum and minimum fields. The difference between these two quasiequilibrium states provides a lower limit of N_v. In the downward channel in Fig. 2, most vortices in cages no. 1 to no. 4 were rectified. The higher the maximum field is, the higher the vortex density in the cages (especially in no. 1 and no. 2) and the resulting N_v are. In this sense, the behavior of N_v, observed in Fig. 3, is naturally understood.

It is noteworthy to compare our results with those in Ref. [8], which were taken under an ac driven current, at frequencies between 500 Hz and 10 kHz. As also seen in [3,17,18], when the frequency increases, the distance over which vortices move during one cycle becomes shorter. Indeed, particles moved from one pinning well to a neigh-

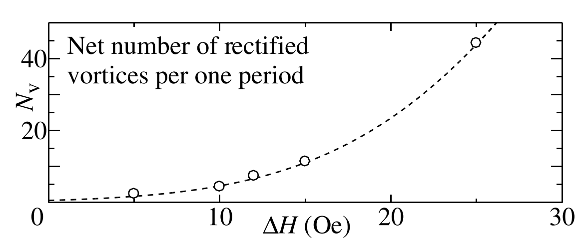

FIG. 3. Net number of rectified vortices N_v transported downward from cage no. 3 to no. 4 versus the amplitude, ΔH, in one period of the field, at 6.9 K, and with $H_{min} = 15$ Oe, as in Fig. 1(c). The dotted line is just a guide for the eye.

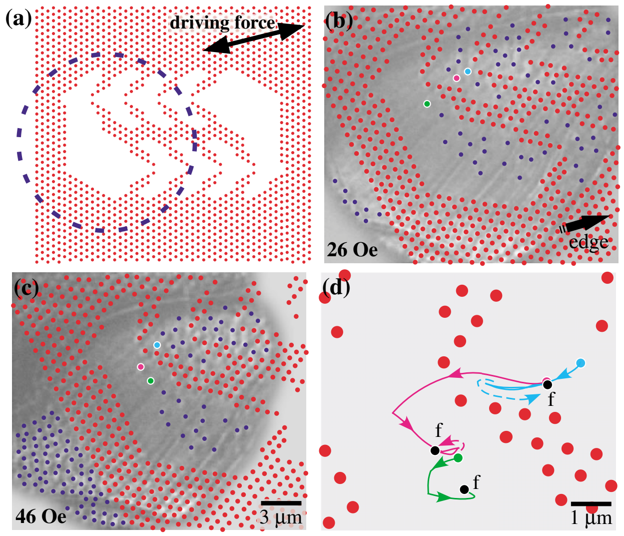

FIG. 4 (color). (a) Pinning site locations (red dots) of a closed circuit channel. Characteristic lengths are the same as those in Fig. 1(a). (b),(c) Sequence of snapshots taken at 6.5 K when increasing H from 26 to 46 Oe. Pinned and unpinned vortices are represented by red and blue circles, respectively. The green (light blue) vortex was the first (last) rectified vortex four cycles prior to (after) these snapshots monitoring the tagged magenta vortex. The field of view in (b) and (c) is inside the blue dashed circle in (a). The arrows in (a) show the direction of the driving force exerted by the oscillating H. With increasing H, vortices were driven to the left. (d) Trajectories of three vortices in this field cycle (26 Oe ↔ 46 Oe). Black dots indicate the final locations of the three vortices.

boring trap in one cycle at high frequencies [5,8,17,18]. However, in our experimental observation at much lower frequencies, once vortices escape from one potential energy cage in the channel, most of the vortices traveled longitudinally through the channel all the way to the outside without stopping at another cage, as in the low-frequency limit in [3]. Therefore, the flux-gradient-driven vortex dynamics at low frequencies in our experiment is quite different from the current-driven dynamics at high frequencies in Ref. [8]. Our experiment provides direct insight into a very different way of controlling the motion of vortices in superconductors.

In our experiments, the number of vortices in the system was altered by changing the applied magnetic field. Thus, our system in Fig. 2 is an open system where the total number of vortices is a variable. To illustrate a different way to control the motion of vortices, we made a "closed loop" [see Fig. 4(a)] where the number of vortices was fixed because these cannot escape through the (red) regions with pinned vortices. The rectification of vortices in a closed system provides a novel demonstration of the ability to control the motion in 2D channels, where the vortex path can bend and take turns [3] as opposed to just moving along one (or several adjacent parallel) linear 1D track(s). Snapshots when increasing H are shown in Figs. 4(b) and 4(c). The initial state was prepared using the field-cooling process described above. H was periodically oscillated between 26 and 46 Oe. The vortices inside the loop were exposed, via the long-range Pearl potential, to a time-dependent field gradient (i.e., a force) produced by the variations of $B(t)$ outside the pinned vortex area (which was located near the sample edge). This drove the inner vortices. With increasing H from 26 Oe [Fig. 4(b)] to 46 Oe [Fig. 4(c)], one (magenta) vortex was pushed southwest out of the front cage of the channel directed to the left, and began to turn around toward another channel directed the opposite way. The trajectory of this vortex in this field cycle is shown in Fig. 4(d). In this (nonoptimized) regime of parameters, the net motion of vortices in each cycle was small. We observed such rectification of vortices every four cycles of changing H in three parts out of four funnels connecting straight channels and curved regions. The rectified motion of vortices in one of these funnels are illustrated in Figs. 4(b)–4(d). A rough estimate (not a direct observation) indicates that after 350 cycles vortices should go through the loop.

The transport of oscillatory field-gradient-driven vortices observed in this closed loop suggests novel ways to transport vortices one by one along curved paths, including cyclic vortex "conveyor belts" and pumps [3,6,18]. Also, the energy of vortices moving in circles could be extracted as a dc voltage output along a radial direction.

We thank S. Savel'ev for fruitful discussions, and N. Moriya for technical support.

*Electronic address: ytogawa@harl.hitachi.co.jp

[1] See, e.g., R. D. Astumian and P. Hänggi, Phys. Today **55**, No. 11, 33 (2002).
[2] C.-S. Lee *et al.*, Nature (London) **400**, 337 (1999).
[3] J. F. Wambaugh *et al.*, Phys. Rev. Lett. **83**, 5106 (1999).
[4] C. J. Olson *et al.*, Phys. Rev. Lett. **87**, 177002 (2001).
[5] B. Y. Zhu *et al.*, Phys. Rev. B **68**, 014514 (2003).
[6] S. Savel'ev and F. Nori, Nat. Mater. **1**, 179 (2002).
[7] W. K. Kwok *et al.*, Physica (Amsterdam) **382C**, 137 (2002).
[8] J. E. Villegas *et al.*, Science **302**, 1188 (2003).
[9] D. D. Morrison and R. M. Rose, Phys. Rev. Lett. **25**, 356 (1970).
[10] K. Harada *et al.*, Nature (London) **360**, 51 (1992).
[11] A short video clip of vortices moving through cages is available at http://dml.riken.go.jp/~nori/togawa/.
[12] T. Matsuda *et al.*, Science **271**, 1393 (1996).
[13] K. Harada *et al.*, Science **274**, 1167 (1996).
[14] J. Pearl, Appl. Phys. Lett. **5**, 65 (1964); P. Martinoli, Phys. Rev. B **17**, 1175 (1978).
[15] A. Tonomura *et al.*, Nature (London) **412**, 620 (2001).
[16] S. Mathias and F. Mueller, Nature (London) **424**, 53 (2003).
[17] S. Savel'ev *et al.*, Phys. Rev. Lett. **91**, 010601 (2003).
[18] B. Y. Zhu *et al.*, Phys. Rev. Lett. **92**, 180602 (2004).